Mutations in the gene encoding the basal body protein RPGRIP1L, a nephrocystin-4 interactor, cause Joubert syndrome

Heleen H Arts[1,8], Dan Doherty[2,8], Sylvia E C van Beersum[1], Melissa A Parisi[2], Stef J F Letteboer[1], Nicholas T Gorden[2], Theo A Peters[3], Tina Märker[4], Krysta Voesenek[1], Aileen Kartono[1], Hamit Ozyurek[5], Federico M Farin[6], Hester Y Kroes[7], Uwe Wolfrum[4], Han G Brunner[1], Frans P M Cremers[1], Ian A Glass[2], Nine V A M Knoers[1] & Ronald Roepman[1]

Protein-protein interaction analyses have uncovered a ciliary and basal body protein network that, when disrupted, can result in nephronophthisis (NPHP), Leber congenital amaurosis, Senior-Løken syndrome (SLSN) or Joubert syndrome (JBTS)[1–6]. However, details of the molecular mechanisms underlying these disorders remain poorly understood. RPGRIP1-like protein (RPGRIP1L) is a homolog of RPGRIP1 (RPGR-interacting protein 1), a ciliary protein defective in Leber congenital amaurosis[7,8]. We show that RPGRIP1L interacts with nephrocystin-4 and that mutations in the gene encoding nephrocystin-4 (*NPHP4*) that are known to cause SLSN disrupt this interaction. *RPGRIP1L* is ubiquitously expressed, and its protein product localizes to basal bodies. Therefore, we analyzed *RPGRIP1L* as a candidate gene for JBTS and identified loss-of-function mutations in three families with typical JBTS, including the characteristic mid-hindbrain malformation. This work identifies *RPGRIP1L* as a gene responsible for JBTS and establishes a central role for cilia and basal bodies in the pathophysiology of this disorder.

Cerebello-oculo-renal syndromes (CORS), which include JBTS, are a group of autosomal recessive disorders characterized by the variable association of brain, kidney and eye abnormalities[9,10]. These syndromes share a complex brainstem malformation often referred to as the 'molar tooth sign' (MTS) owing to its appearance on axial magnetic resonance imaging (MRI). The MTS is characterized by cerebellar vermis hypoplasia or aplasia; elongated, thickened and maloriented superior cerebellar peduncles and a deep interpeduncular fossa[11]. The phenotypic presentation of CORS is heterogeneous and includes renal abnormalities (cystic dysplastic kidneys or juvenile nephronophthisis) that may be asymptomatic or mildly symptomatic until adolescence, when chronic renal failure may occur. Neurological features include developmental delay, hypotonia, ataxia, oculomotor apraxia, nystagmus and abnormal respiratory control, mainly in neonates. Ocular abnormalities vary and can include chorioretinal colobomas, progressive retinopathies or even congenital blindness. Other abnormalities include hepatic fibrosis, polydactyly, tongue tumors and central nervous system malformations. Core diagnostic features of CORS have been identified, but incomplete and overlapping phenotypes are often described, as well as phenotypic variability within families[9,12].

Recently, four genes associated with JBTS have been identified: *NPHP1* at 2q13 (ref. 5), *AHI1* at 6q23.3 (ref. 13), *CEP290* (*NPHP6*) at 12q21.3 (ref. 4) and the Meckel-Gruber syndrome–associated gene *TMEM67* (*MKS3*) at 8q22.1 (ref. 14). Mutations in these genes together account for a minority of cases of JBTS. *NPHP1* (ref. 15), *CEP290* (ref. 16) and *TMEM67* (ref. 17) encode members of a complex network of ciliary and basal body proteins (including the NPHP protein family) that, when disrupted, result in features of the CORS phenotype. We demonstrated that RPGRIP1, a member of the protein complex in connecting cilia of photoreceptors that is associated with CEP290[18], binds directly to nephrocystin-4, a protein that in turn interacts with the *NPHP1* gene product nephrocystin[1,3]. Mutations in the gene encoding nephrocystin-4, *NPHP4*, can cause nephronophthisis or a combination of nephronophthisis and progressive retinal degeneration known as SLSN[1,19].

Homology searches of EST databases with RPGRIP1 uncovered a single homolog that has 29% amino acid identity, RPGRIP1L, encoded by the *RPGRIP1L* gene (previously called *KIAA1005*) at 16q12.2 (**Fig. 1a**). The greatest degree of similarity (52% identity) is

[1]Department of Human Genetics, Radboud University Nijmegen Medical Centre and Nijmegen Centre for Molecular Life Sciences, 6500 HB Nijmegen, The Netherlands. [2]Department of Pediatrics, University of Washington School of Medicine, Seattle, Washington 98195-6320, USA. [3]Department of Otorhinolaryngology, Radboud University Nijmegen Medical Centre, 6500 HB Nijmegen, The Netherlands. [4]Institut für Zoologie, Johannes Gutenberg University, D-55099 Mainz, Germany. [5]Department of Pediatrics, Ondokuz Mayis University, 55139 Kurupelit/Samsun, Turkey. [6]Department of Environmental and Occupational Health Sciences, School of Public Health, University of Washington, Seattle, Washington 98195-7234, USA. [7]Division of Biomedical Genetics, University Medical Center Utrecht, 3508 AB Utrecht, The Netherlands. [8]These authors contributed equally to this work. Correspondence should be addressed to R.R. (r.roepman@antrg.umcn.nl).
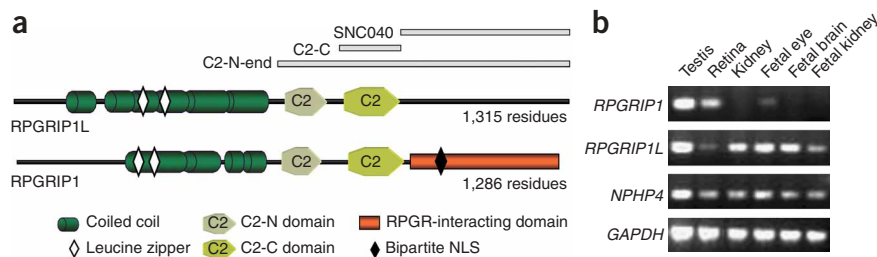
Figure 1 Structure of RPGRIP1L and RPGRIP1 and their mRNA expression in different tissues. (**a**) Structure of the full-length human RPGRIP1L and RPGRIP1 protein homologs. Gray bars at the top denote RPGRIP1L protein segments used for antibody generation (SNC040) and recombinant protein expression (C2-C and C2-N-end). (**b**) RT-PCR analysis of *RPGRIP1*, *RPGRIP1L* and *NPHP4* using mRNA from indicated tissues. The ubiquitously expressed *GAPDH* gene was used as a positive control.

found in the central protein kinase C conserved region (C2 domain), which, in RPGRIP1, binds to nephrocystin-4 (ref. 3). Expression analysis showed a more ubiquitous expression pattern of *RPGRIP1L* compared with *RPGRIP1*, including prominent expression in the fetal eye, brain and kidney (**Fig. 1b**). These findings prompted us to analyze whether RPGRIP1L, similar to its homolog RPGRIP1, could also be a member of the ciliary/basal body protein network in other tissues affected by CORS, such as brain and kidney.

Reciprocal glutathione *S*-transferase pull-down analysis (**Fig. 2a** and **Supplementary Fig. 1** online) and coimmunoprecipitation experiments (**Fig. 2b**) showed that the C2-C domain of RPGRIP1L indeed interacts with nephrocystin-4. In addition, nephronophthisis- and SLSN-associated mutations in *NPHP4* (G754R and Q779X) disrupt this interaction, whereas polymorphisms (R740H and

R848W) do not affect the binding (**Fig. 2c**), as previously reported for the RPGRIP1-nephrocystin-4 interaction[3].

We determined subcellular localization in mammalian cells using variants of green fluorescent protein (GFP) fused to recombinant nephrocystin-4 (full-length) and RPGRIP1L (the N-terminal part without coiled-coil domains; **Fig. 3a–e**). In single transfected COS-1 cells, nephrocystin-4 localized to the centrosome (**Fig. 3a**), whereas RPGRIP1L was dispersed throughout the cytoplasm (**Fig. 3b**). Cotransfection of both proteins showed that nephrocystin-4 was able to recruit RPGRIP1L to the centrosome (**Fig. 3c–e** and **Supplementary Fig. 2** online).

To assess the endogenous protein expression and localization, we raised a polyclonal antibody against RPGRIP1L (SNC040) and confirmed its specificity (**Supplementary Fig. 3** and **Supplementary Fig. 4** online). We used this antibody together with anti-acetylated α-tubulin, anti-γ-tubulin, anti-ninein and anti-nephrocystin-4 to stain ARPE19 cells that carry primary cilia. This showed that RPGRIP1L is localized to the basal body at the base of these cilia, where it colocalizes with nephrocystin-4 (**Fig. 3f–i**).

In cryosections of rat retinas, antibodies to RPGRIP1L stained connecting cilia and the cell bodies of photoreceptors as well as synapses in the outer plexiform layer, a pattern largely coinciding with anti-nephrocystin-4 staining (**Fig. 4a–f** and **Supplementary Fig. 5** online). In the inner nuclear layer, the centrosomes were stained in a punctate pattern (**Fig. 4g–i**). We confirmed the ciliary localization

Figure 2 RPGRIP1L interaction with nephrocystin-4. (**a**) GST pulldown analysis of recombinant RPGRIP1L and nephrocystin-4 (N4). Lanes 3 and 6 show that Flag-tagged N4[591-1093] (65-kDa band) is efficiently pulled down by GST-fused RPGRIP1L[C2-N-end] and by the C-terminal C2 domain of RPGRIP1L. The mock-transfected cell lysates do not show a signal (lanes 1 and 4). RPGRIP1L weakly interacts with itself: note thin band of Flag-tagged RPGRIP1L[C2-N-end] at 90 kDa (lanes 2 and 5). (**b**) Coimmunoprecipitation of RPGRIP1L and nephrocystin-4 (N4). Flag-tagged RPGRIP1L[C2-N-end] (90 kDa) coimmuno-precipitated with the HA-tagged N4[FL] (160 kDa) (lane 1). The negative control, Flag-tagged leucine-rich repeat kinase-2 fragment (LRKK2[LRR]) (45 kDa), does not coimmuno-precipitate with HA-N4[FL], indicating that the coimmunoprecipitation of RPGRIP1L[C2-N-end] (lane 1) was specific. RPGRIP1L[C2-N-end] immunoprecipitates with N4[FL] but not with anti-HA beads alone, again supporting the interaction between RPGRIP1L and nephrocystin-4 (lane 3). The middle two blots show 10% input of the COS-1 lysate protein mixtures as well as immunoprecipitation of HA-tagged nephrocystin-4 with anti-HA beads. (**c**) Yeast two-hybrid analysis demonstrates *in vitro* binding between RPGRIP1L and nephrocystin-4 (N4). The C-terminal C2 domain of RPGRIP1L and the central nephrocystin-4 fragment (residues 591–1093, known to bind to RPGRIP1) were fused to GAL4-BD and GAL4-AD domains, respectively, and protein-protein interaction was confirmed in a liquid β–galactosidase activity assay (N4_wt). Binding with the C2 domain of RPGRIP1L was severely disrupted when the nephrocystin-4 fragment contained SLSN-associated mutations (G754R and Q779X)[3]. In contrast, polymorphisms in nephrocystin-4 (R740H and R848W)[3] did not show any effect. The error bars show s.d.
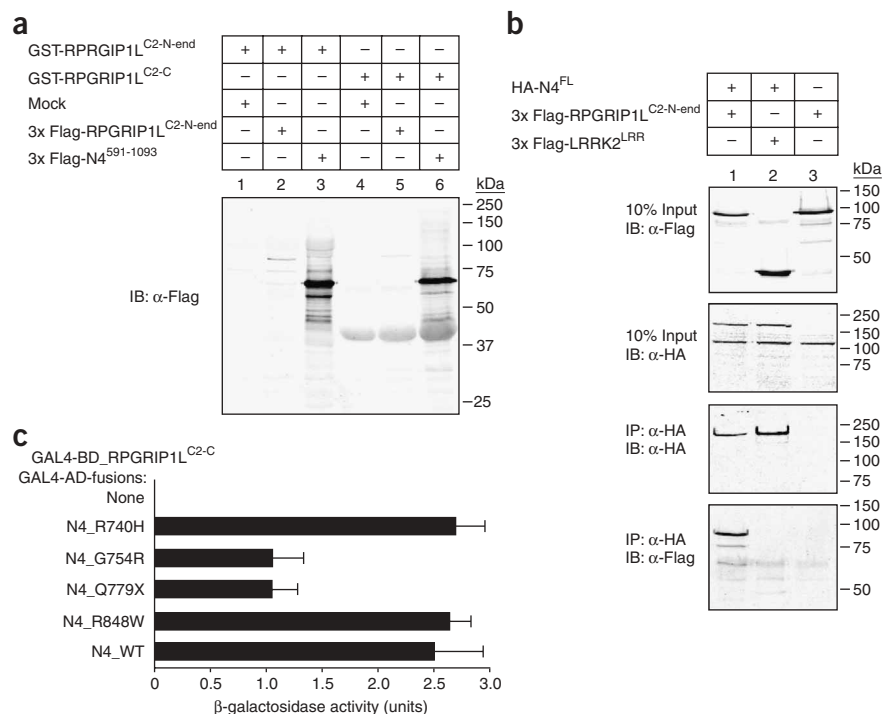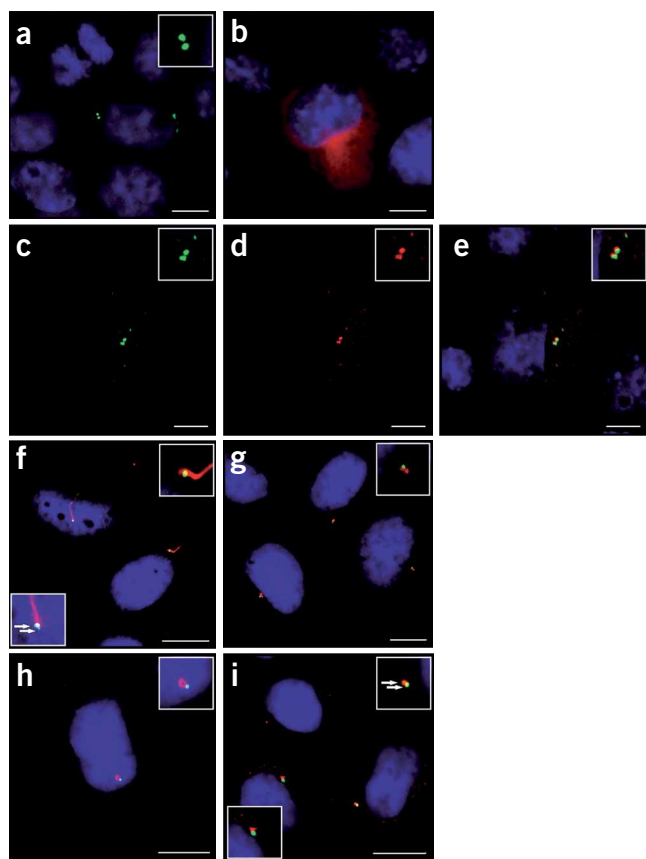
Figure 3 Colocalization of RPGRIP1L and nephrocystin-4 in the basal bodies of mammalian cells. (**a–e**) Colocalization of recombinant mRFP-RPGRIP1L[C2-N-end] and eCFP-nephrocystin-4[FL] in COS-1 cells. (**a**) eCFP-Nephrocystin-4[FL] (green) localized to the centrosome in single transfected cells. (**b**) mRFP-RPGRIP1L[C2-N-end] (red) stained the cytoplasm in single transfected cells. (**c–e**) eCFP-nephrocystin4[FL] (green) recruited mRFP-RPGRIP1L[C2-N-end] (red) to the centrosome. (**f–i**) RPGRIP1L associated with the basal body in ciliated ARPE19 cells. (**f**) Costaining using anti-RPGRIP1L (green) and anti-acetylated α-tubulin (red) showed that RPGRIP1L is located at the base of cilia, the basal body. (**g**) RPGRIP1L (green) is localized in close association with ninein (red), (**h**) γ-tubulin (red) and (**i**) nephrocystin-4 (red). In some cases, the RPGRIP1L signal appeared in two dots at the base of the cilium (arrows in insets). Incomplete colocalization with γ-tubulin at these subcellular sites suggests that RPGRIP1L could be associated with the distal or subdistal appendages of the mother centriole, similar to the situation of the centrosomal protein ninein[30]. Blue: DAPI staining of the nuclei. Scale bars: 10 μm in all images.

body localization. We also detected islands of RPGRIP1L staining in the choroid plexus, a tissue important in the regulation of cerebrospinal fluid[23] (**Fig. 5g–i**). Again, we found colocalization with CEP290 in this brain region (data not shown). In the kidney, we observed colocalization of RPGRIP1L with CEP290 (**Fig. 5j–l**) and nephrocystin-4 (**Fig. 5m–o**) at the basal bodies of renal tubular cilia.

Based on RPGRIP1L's expression and localization to cilia and basal bodies in the retina, kidney and brain, its interaction with nephrocystin-4 and its colocalization with CEP290, we hypothesized that mutations in *RPGRIP1L* might cause JBTS in a subset of affected individuals. To identify appropriate families for sequence analysis, we genotyped affected and unaffected siblings in our cohort of consanguineous families with JBTS using the Affymetrix GeneChip Human Mapping 50K Array Xba 240. We used a cutoff of 80 consecutive homozygous SNPs to identify candidate regions of loss of heterozygosity (LOH) in the offspring of first cousins. Three families showed LOH at 16q12.2 (**Fig. 6a** and **Supplementary Table 1** online). Sequencing the 26 coding exons and the intron-exon boundaries showed homozygous loss-of-function mutations in two Turkish families (**Fig. 6b**): 2305-1G>A in UW42 (splice site mutation predicted to result in a frameshift) and 1721delA in UW43 (frameshift mutation), both predicted to cause premature protein truncation before the C2 domains. As expected, the parents were heterozygous for the mutations. At 3 and 10 years of age, the affected probands
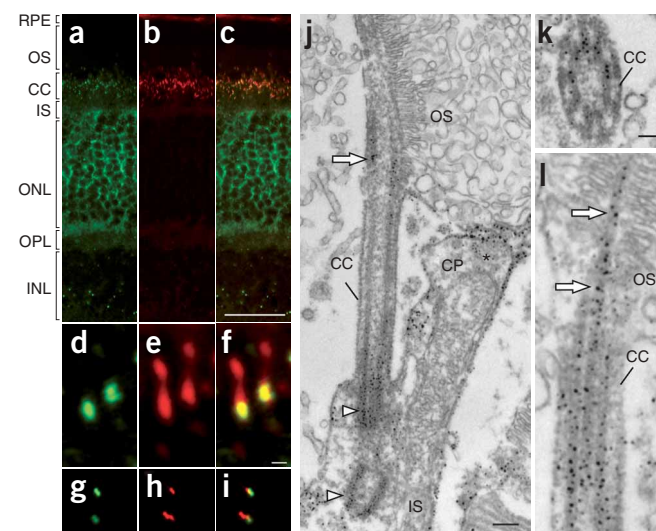
of RPGRIP1L by double-labeling with anti-centrin, a specific marker for the connecting cilium of photoreceptors[20] (**Fig. 4d–f**). Higher-resolution analyses by immunoelectron microscopy allowed us to localize RPGRIP1L to the basal bodies and ciliary axoneme of the connecting cilium (**Fig. 4j–l**). Furthermore, the apical area of calycal processes of the photoreceptors was stained by anti-RPGRIP1L (**Fig. 4j**). Little is known about the function of this subcellular domain. As a photoreceptor-specific protocadherin is also present in this region[21], this domain may provide mechanical support for disk morphogenesis by specific membrane-membrane adhesion, in which RPGRIP1L may participate.

In rat brain, RPGRIP1L is specifically localized in islands of dots on the apical side of ependymal cells that have tufts of cilia and line the ventricles and interventricular connections (**Fig. 5a–f**). Costaining of CEP290 (**Fig. 5a–c**) and polaris[22] (**Fig. 5d–f**) confirmed basal

Figure 4 Localization of RPGRIP1L in the retina. (**a–i**) Double immunostaining of RPGRIP1L (green) and pan-centrin (red, connecting cilium (CC) marker) in rat retinal cryosections demonstrated that RPGRIP1L is expressed in multiple cell layers of the retina and localized to the CC of photoreceptor cells (**a–c**). Higher magnification shows focal localization at the base of the CC (**d–f**). In addition, we observed partial colocalization for RPGRIP1L and centrin in one centriole of the centrosomes in the inner nuclear layer (INL) (**g–i**). RPE, retinal pigment epithelium; OS, outer segments; IS, inner segments; ONL, outer nuclear layer; OPL, outer plexiform layer. (**j–l**) Immunoelectron microscopy showed that RPGRIP1L is associated with the plasma membrane and localized in the basal body complex (arrowheads), the CC, the axonemal microtubules projecting into the OS (arrows) and calycal processes (CP, asterisk) of photoreceptors. Scale bars represent 20 μm in **a–c**; 0.2 μm in **d–f**, **j** and **l**; 0.5 μm in **g–i** and 0.1 μm in **k**.

Figure 5 Localization of RPGRIP1L in brain and kidney. (**a**–**f**) Immuno-staining of RPGRIP1L, CEP290, polaris and CK18 (choroid plexus marker) in cryosections of the rat brain. (**a**,**d**) RPGRIP1L (green) immunolocalized in islands of dots that line the ventricles. Costaining of CEP290 (**b**, red) and polaris/IFT88 (**e**, red) demonstrates that both of these proteins colocalize perfectly with RPGRIP1L at the basal bodies of the ependymal cilia (**c** and **f**, overlays), for which polaris was used as a marker[22]. (**g**–**i**) Costaining of RPGRIP1L (green) with CK18 (red) that stains the ependymal cells of the choroid plexus. (**j**–**o**) Colocalization of RPGRIP1L, CEP290 and nephrocystin-4 in the kidney. (**j**) RPGRIP1L (green) localizes mainly in the basal bodies of the primary cilia of renal tubule cells (arrows), where it colocalizes with CEP290 (**k**, red; **l**, overlay). (**m**–**o**) Very similarly, RPGRIP1L (**m**, green) and nephrocystin-4 (**n**, red) also colocalize at the ciliary basal bodies (**o**, overlay). Insets show a magnification of a primary cilium in the renal tubule. Scale bars represent 10 μm.
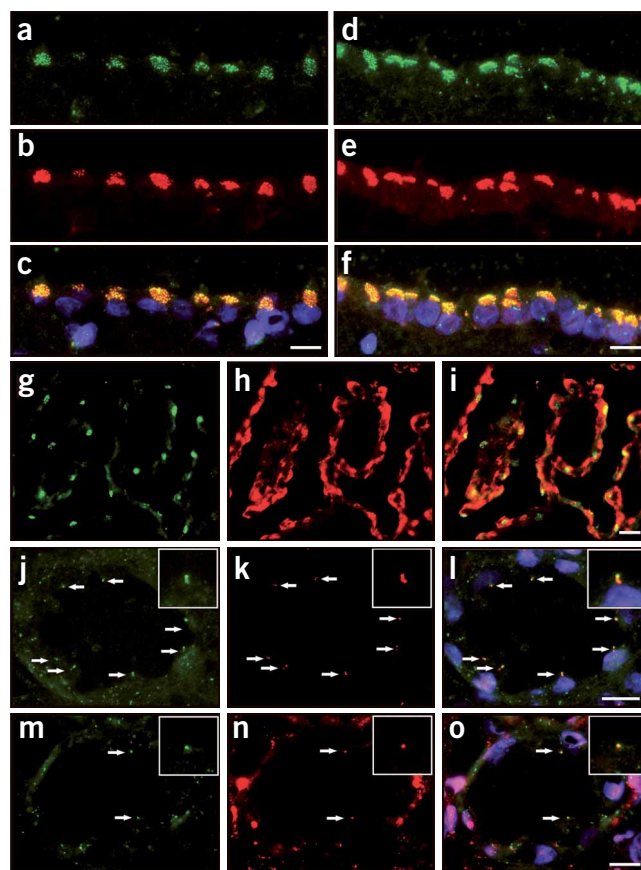
showed the MTS on MRI, ataxia, developmental delay and abnormal eye movements but no retinal disease by electroretinogram. The younger child has normal renal function, and the older child has renal failure requiring dialysis. We did not identify any mutations in the third family.

To identify additional mutations, we genotyped microsatellite markers around the *RPGRIP1L* gene in our multiplex, non-consanguineous families. We excluded *RPGRIP1L* as a candidate gene when the microsatellite markers were fully informative and identical in affected and unaffected siblings. We were unable to exclude 14 families, and we found mutations in one of them (**Supplementary Table 1**). In UW15, a non-consanguineous family of mixed Northern European descent, we identified compound heterozygous mutations: one nonsense (2050C>T; Q684X, predicted to truncate the protein before the C2 domains) and one missense (1843A>C; T615P; **Fig. 6a,b** and **Supplementary Table 1**). Each parent was heterozygous for one of the mutations, and we did not identify the nucleotide change in 200 ethnically matched chromosomes. The missense mutation was predicted not to be tolerated using the Sort Intolerant from Tolerant (SIFT)[24] algorithm and was predicted to be possibly damaging using the Polymorphism Phenotype (PolyPhen) algorithm[25]. We found that both mutations in pedigree UW15 severely disrupt nephrocystin-4 binding (**Supplementary Fig. 6** online). Brain MRI showed the MTS in both affected children (**Fig. 6c**), and UW15 II:3 had a small occipital encephalocele. Both children also showed developmental delay, dysmorphic features, abnormal eye movements, strabismus, bilateral ptosis and postaxial hand polydactyly. Neither had retinal dystrophy on examination, but we could not completely exclude retinal dysfunction by visual evoked potential testing in UW15 II:3. This subject is now 5 years of age and does not have evidence of renal disease, based on normal renal ultrasound, BUN, Cr and urinalysis results. UW15 II:2 died from central apnea at 1 year of age. The phenotype in UW15 overlaps with Meckel-Gruber syndrome, with one affected child having an occipital encephalocele and both having postaxial polydactyly. In contrast to classic Meckel-Gruber syndrome, these children did not have congenital polycystic kidneys. However, given the broad phenotypic heterogeneity observed in CORS, recently illustrated by the mixed JBTS–MKS phenotypes resulting from *MKS3* mutations[14], we argue that *RPGRIP1L* is also an MKS candidate gene.

In summary, we identified loss-of-function mutations in 3 of 68 multiplex and consanguineous families with JBTS, indicating that *RPGRIP1L* accounts for ~5% of JBTS cases in our cohort. This work identifies *RPGRIP1L* as a gene responsible for JBTS and further establishes a central role for cilia and basal bodies in the pathophysiology of CORS, as the gene product is localized to basal

bodies in brain, retina and kidney tissues. RPGRIP1L is required for normal brain development and kidney function, as mutations in this gene cause developmental delay, ataxia, abnormal eye movements and renal disease. In contrast to subjects with loss-of-function *RPGRIP1* mutations, our subjects with *RPGRIP1L* mutations develop renal but not retinal disease. These phenotypic differences, in spite of marked sequence similarity, may indicate that RPGRIP1L and RPGRIP1 have partially redundant roles in different cell types.

METHODS

Subjects. Subjects in this study were recruited worldwide and collected under the approval of the Human Subjects Division at the University of Washington. Characteristic brain imaging findings (the MTS) combined with developmental delay and ataxia were the minimal criteria for JBTS. Cerebellar vermis hypoplasia was a sufficient imaging criterion in subjects not evaluated by MRI. Known genes and loci for JBTS (*AHI1*, *CEP290*, *NPHP1*, *MKS3*, chromosomal loci 9q34 and 11p11.2–q12.1) were excluded in the consanguineous families by either haplotype analysis using microsatellite markers or direct sequencing, with the exception of the chromosome 11p11.2–q12.1 locus in UW42.

SNP and microsatellite marker genotyping. SNPs were genotyped using the GeneChip Human Mapping 50K Array Xba 240 (Affymetrix) under standard conditions. Microsatellite markers at chromosome 16q12.2 were genotyped using ABI primers and an ABI PRISM 3100 Genetic Analyzer (Applied Biosystems).

DNA sequencing. Sequencing was performed using standard techniques and an ABI PRISM 3100 Genetic Analyzer (Applied Biosystems). Forward and reverse strands of all 26 exons were sequenced. Approximately 30 bp of intronic
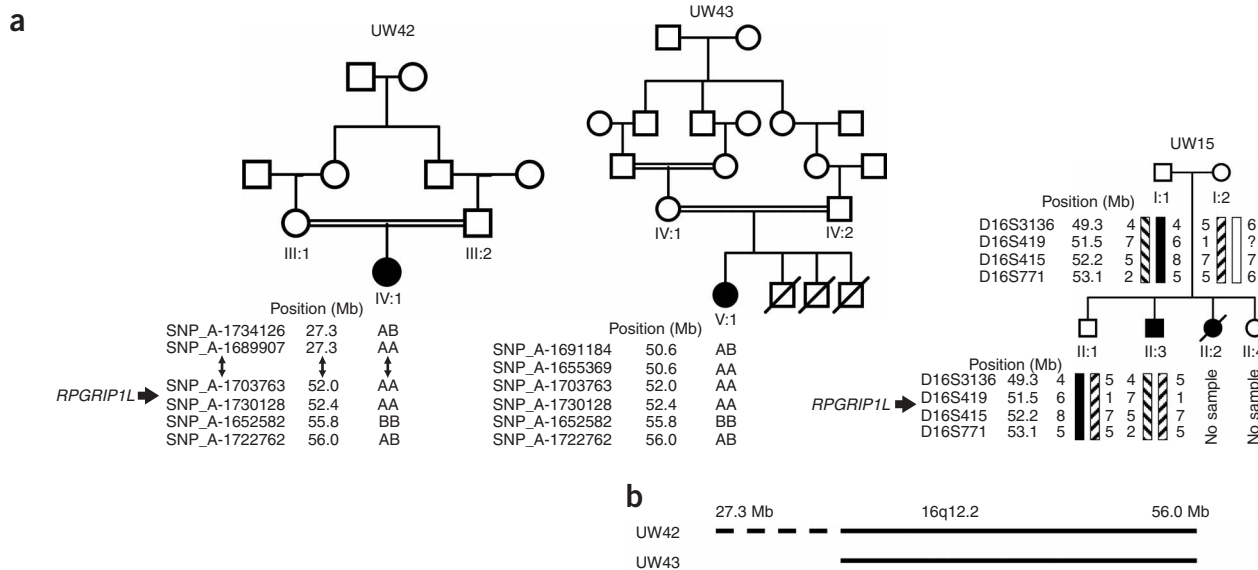
Figure 6 Mapping and sequence analysis of families carrying *RPGRIP1L* mutations. (**a**) SNP and microsatellite alleles flanking the *RPGRIP1L* gene in consanguineous (UW42, UW43) and multiplex (UW15) pedigrees. The positions of the SNP markers on chromosome 16 are indicated in Mb, with the corresponding alleles designated by A and B. AA or BB indicates that the proband is homozygous for SNP markers that surround the *RPGRIP1L* gene (the position is shown by an arrow). Double-headed arrows indicate a long stretch of homozygous markers. For pedigree UW15, the alleles generated by microsatellite markers surrounding *RPGRIP1L* are shown. (**b**) Diagram of chromosome 16q12.2 in the region of *RPGRIP1L*, with regions of homozygous markers for probands from UW42 and UW43 indicated by horizontal bars. The expanded diagram of the *RPGRIP1L* gene with exons indicated by hatch marks and relative locations of nonsense (UW42, UW43, UW15) and missense (UW15) mutations shown below. Sequence traces for the probands (IV:1 in UW42, V:1 in UW43, and II:3 in UW15) and heterozygous parent in UW43 IV:1 demonstrate each mutation, shown in red relative to wild-type sequence (red arrows). (**c**) Axial and mid-sagittal MRI images from UW15 II:2 show the classic MTS, with severe cerebellar vermis hypoplasia, horizontally oriented, elongated superior cerebellar peduncles and deep interpeduncular fossa.
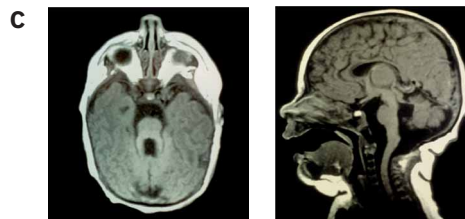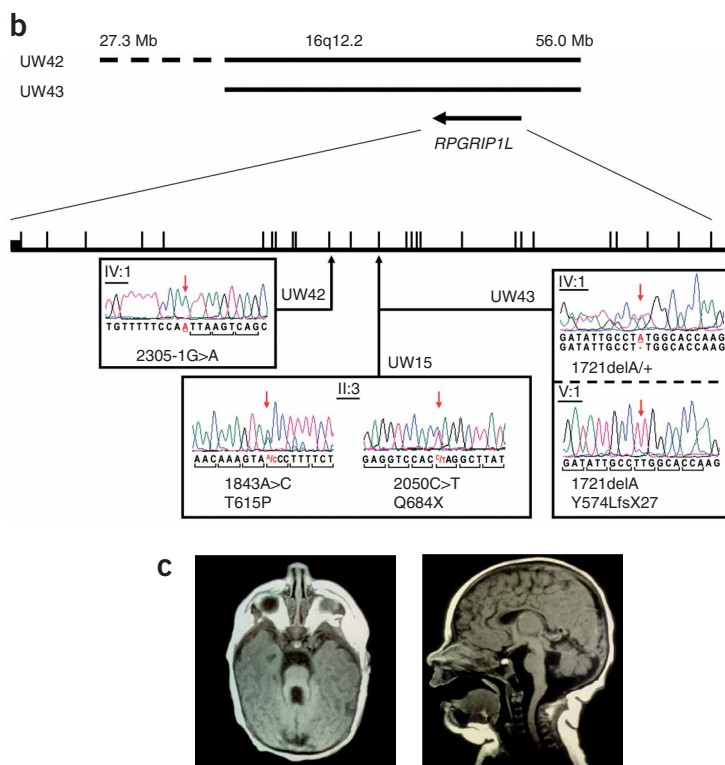
sequence was included upstream and downstream of each exon. Primers and conditions used are depicted in **Supplementary Table 2** online.

RT-PCR. Human adult or fetal mRNA was isolated using the Oligotex mRNA kit (QIAgen), and RT-PCR analysis of *RPGRIP1*, *RPGRIP1L* and *NPHP4* was performed using RNA from testis, retina, kidney, fetal eye, fetal brain and fetal kidney tissues. The primers are depicted in **Supplementary Table 2**. Amplification was carried out in PCR buffer containing 2 mM $MgCl_2$ (30 cycles of denaturation for 30 s at 96 °C, annealing for 30 s at 60 °C and extension for 35 s at 72 °C, with an initial denaturation step for 2 min at 98 °C). The products were analyzed on a 1.5% agarose gel.

DNA constructs. cDNA clones KIAA1005 and KIAA0673 were obtained from the Kazusa DNA Research Institute. Gateway-adapted expression constructs were created using the Gateway cloning system (Invitrogen), and expression vectors used were previously described[3]. All PCR-generated fragments were verified by nucleotide sequencing. Mutations were introduced using the QuikChange site-directed mutagenesis kit (Stratagene). Using Gateway-adapted PCR, we amplified RPGRIP1L[C2-N-end] (amino acid residues 411–1055 of GenBank entry BAA76849), RPGRIP1L[SNC040] (amino acid residues 717–1055 of GenBank entry BAA76849), RPGRIP1L[C2-C] (amino acid residues 591–746 of GenBank entry BAA76849). Construction of N4[FL]/ENTR and N4[591–1093] were previously described[3].

Coimmunoprecipitation. The following constructs were used for the co-immunoprecipitation experiment: pcDNA3-HA-N4[FL]/EXP (N-terminal hemagglutinin (HA) tag), p3×Flag-RPGRIP1L[C2-N-end]/EXP (N-terminal 3× Flag-tag) and p3×Flag-LRRK2[LRR]/EXP as a control plasmid. Transfection of COS-1 cells was performed as previously described[3]. Proteins were expressed for 24 h, and cells were subsequently washed in PBS and lysed in ice-cold lysis buffer (50 mM Tris-HCl (pH 7.5), 150 mM NaCl, 0.5% Triton X-100 and complete protease inhibitor cocktail from Roche). Lysates were cleared by centrifugation at 4 °C for 10 min at 14,000*g*. Immunoprecipitation was performed with anti-HA affinity matrix (Roche) overnight at 4 °C. Beads were

then washed four times with lysis buffer, mixed with Laemmli Sample Buffer (BioRad) and boiled for 5 min at 95 °C. The immunocomplexes were then analyzed with SDS-PAGE followed by protein blot analysis with tag-specific primary antibodies: monoclonal mouse antibody to Flag (1:1,000, clone M2, Sigma) and anti-HA monoclonal mouse antibody (1:1,000, clone HA-7, Sigma).

GST pulldown. BL21-DE3 cells were transformed with pGEX-KG-RPGRIP1L[C2-N-end]/EXP, pGEX-KG-RPGRIP1L[C2C]/EXP, or pGEX-KG-N4[591-1093]/EXP. The produced fusion proteins have a GST tag at the N terminus. Purification of the GST fusion proteins was performed as previously described[26]. In the GST pulldown procedure, 50 μl of the GST fusion protein and 100 μl COS-1 cell lysates expressing either Flag-tagged RPGRIP1L or nephrocystin-4 proteins were used as protein input. We used 50 μl of glutathione Sepharose 4B beads (Amersham Biosciences) per pulldown reaction. In all the washing solutions described below, a protease inhibitor cocktail (Roche) was added. Before incubation with the GST fusion protein, the beads were washed twice with TBS (25 mM Tris (pH 7.4) and 150 mM NaCl). Washing of the beads was followed by a 2-h incubation of the GST fusion protein with the beads. After this incubation, the beads were washed with TBSTD buffer (25 mM Tris (pH 7.4), 150 mM NaCl, 1.0% Triton X-100 and 2 mM DTT). The Sepharose beads with the bound GST or GST-fusion proteins were then incubated with the COS-1 cell lysates expressing either Flag-tagged RPGRIP1L or nephrocystin-4 proteins overnight at 4 °C. After several washes with lysis buffer (50 mM Tris-HCl (pH 7.5), 150 mM NaCl, and 0.5% Triton X-100) and complex washing buffer (50 mM Tris-HCl (pH 7.5), 100 mM NaCl, 2 mM $MgCl_2$, 2 mM $CaCl_2$, 1% Triton X-100 and 2 mM DTT), we added Laemmli Sample Buffer (Biorad) to the beads and analyzed the samples by protein blotting as previously described.

Expression of fluorescent proteins. N4[FL] and RPGRIP1L[C2-N-end] were cloned into the vectors pDest-501 (N-terminal enhanced cyan fluorescent protein (eCFP) tag) and pDest-733 (N-terminal monomeric red fluorescent protein (mRFP) tag). The resulting vectors were transfected in COS-1 cells. Cells were grown overnight on glass microscope slides, fixed in 3.7% paraformaldehyde in PBS and analyzed by fluorescence microscopy as previously described[3].

Protein blotting. COS-1 cells were lysed in 50 mM Tris (pH 7.5), 150 mM NaCl, 0.5% Triton-X100 and passed several times through a needle. Lysates were centrifuged at 20,000g for 30 min at 4 °C. The supernatant (cytosolic fraction) was resolved by SDS-PAGE and analyzed by standard protein blotting techniques. Primary antibodies to Flag and to HA (both from Sigma) were used in a 1:1,000 dilution; monoclonal anti-GFP (Roche, cat. no. 11814460001) was used at 1:1,000; affinity purified anti-RPGRIP1L (SNC040) was used at 1:30,000. Brain tissue was isolated from a 14-d-old female rat and dissolved in extraction buffer (10 mM HEPES (pH 7.9), 10 mM NaCl, 3 mM $MgCl_2$, 1 mM DTT, 1 mM Na_3VO_4 and protease inhibitor cocktail from Roche), using 5 ml buffer per ∼0.5 μg tissue. Tissues were fractionated and subsequently sonicated twice for 30 s. Affinity-purified anti-RPGRIP1L (SNC040) was used at 1:30,000. We used Alexa680 (Molecular Probes) and IRDye800 (Rockland) goat anti-mouse IgG (heavy and light chains (H+L), 1 mg/ml) or goat anti-guinea pig (H+L, 1 mg/ml) as secondary antibodies according to the manufacturer's instructions. PBS with 0.3% Tween-20 was used to wash the blots. Bands were detected and processed using the ODYSSEY application software (Version 1.2, Li-Cor).

Analysis of interactions in yeast. The interactions of the wild-type RPGRIP1L and wild-type and mutant nephrocystin-4 proteins were quantified by determining the β-galactosidase activity using o-nitrophenyl-β-D-galactopyranoside (ONPG) as a substrate as previously described[27].

Immunohistochemistry. Immunohistochemical staining of RPGRIP1L, nephrocystin-4, pan-centrin, acetylated α-tubulin and choroid plexus marker CK18 in cryosections of 14 d-old Wistar rat retina, kidney and brain (all 7 μm) were performed as previously described[28]. We raised a polyclonal antibody in guinea pig against the C-terminal domain of RPGRIP1L that we named SNC040. This antibody was affinity purified with HiTrap NHS-activated HP columns (Amersham Biosciences) according to the manufacturer's instructions.

It was used at a 1:2,000 dilution in all tissue sections. The antibody to nephrocystin-4 (#6, mouse polyclonal)[3] was used at 1:300. The antibody to CK18 (RGE53, mouse monoclonal) was used at 1:3. The antibody to CEP290 (3G4-19, rabbit polyclonal) and the antibody to pan-centrin (20H5, mouse monoclonal) were used at 1:500 and 1:5,000, respectively (see Acknowledgments). The antibody to polaris (BY1700, rabbit polyclonal) was used at 1:500 (see Acknowledgments). Primary antibodies were incubated for 1 h, followed by three washes and a 1-h incubation with the secondary antibody. Secondary antibodies were anti-guinea pig IgG Alexa Fluor 488 and anti-mouse and anti-rabbit IgG Alexa Fluor 568 (all from Molecular Probes); both were used at 1:300. After incubation with the secondary antibodies, sections were washed three times with PBS for 10 min each. Sections were subsequently embedded in Prolong Gold Antifade agent (Invitrogen).

Preembedding immunoelectron microscopy. Labeling was performed as previously described[29]. Vibratome sections through mouse retinas were stained by anti-RPGRIP1L (SNC040) and visualized by appropriate secondary antibodies (Vectastain ABC-Kit, Vector Labs). After fixation with 0.5% OsO_4, specimens were embedded in araldite, and ultrathin sections were analyzed with a FEI Tecnai 12 TEM.

Immunocytochemistry. ARPE19 cells were stained with antibodies to the following proteins: RPGRIP1L (SNC040; 1:500); γ-tubulin (mouse monoclonal, Sigma; 1:1,000; acetylated α-tubulin (mouse monoclonal, Zymed Laboratories; 1:500); nephrocystin-4 #6 (1:50) and ninein (mouse monoclonal; 1:500). ARPE19 cells were seeded on glass slides and grown overnight. Cells were then briefly washed in PBS, fixed in ice-cold methanol for 10 min and blocked with 2% BSA in PBS for 20 min. Slides were then incubated with the primary antibody for 1 h at room temperature and subsequently washed with PBS. Slides were then incubated with secondary antibodies that were previously described. Washing with PBS was repeated. Cells were then embedded in Vectashield with DAPI (Vector Laboratories).

URLs. BLAST and PSI-BLAST: http://www.ncbi.nlm.nih.gov/BLAST/

Accession numbers. GenBank: human RPGRIP1L protein, BAA76849 and *RPGRIP1L* mRNA, NM_015272; human RPGRIP1 protein: NP_065099.

Note: Supplementary information is available on the Nature Genetics website.

AUTHOR CONTRIBUTIONS
The study was designed by N.V.A.M.K. and R.R., who share senior authorship of this paper. H.H.A., S.E.C.v.B., S.J.F.L., T.A.P., T.M., A.K. and U.W. analyzed protein expression and localization; T.M. and U.W. performed immuno-electron microscopy; H.H.A. and S.J.F.L. analyzed protein-protein

interactions; S.E.C.v.B. analyzed gene expression; M.A.P., H.O., H.Y.K. and N.V.A.M.K. acquired clinical data; D.D., N.T.G and F.M.F. performed mapping of microsatellites and SNPs; S.E.C.v.B., N.T.G. and K.V. performed sequence analysis of families; D.D., H.G.B., F.P.M.C., I.A.G., N.V.A.M.K. and R.R. supervised the work and H.H.A., D.D. and R.R. wrote the manuscript, with assistance from most of the coauthors.

1. Mollet, G. *et al.* The gene mutated in juvenile nephronophthisis type 4 encodes a novel protein that interacts with nephrocystin. *Nat. Genet.* **32**, 300–305 (2002).
2. Otto, E.A. *et al.* Nephrocystin-5, a ciliary IQ domain protein, is mutated in Senior-Loken syndrome and interacts with RPGR and calmodulin. *Nat. Genet.* **37**, 282–288 (2005).
3. Roepman, R. *et al.* Interaction of nephrocystin-4 and RPGRIP1 is disrupted by nephronophthisis or Leber congenital amaurosis-associated mutations. *Proc. Natl. Acad. Sci. USA* **102**, 18520–18525 (2005).
4. Sayer, J.A. *et al.* The centrosomal protein nephrocystin-6 is mutated in Joubert syndrome and activates transcription factor ATF4. *Nat. Genet.* **38**, 674–681 (2006).
5. Parisi, M.A. *et al.* The *NPHP1* gene deletion associated with juvenile nephronophthisis is present in a subset of individuals with Joubert syndrome. *Am. J. Hum. Genet.* **75**, 82–91 (2004).
6. den Hollander, A.I. *et al.* Mutations in the *CEP290* (*NPHP6*) gene are a frequent cause of Leber congenital amaurosis. *Am. J. Hum. Genet.* **79**, 556–561 (2006).
7. Roepman, R. *et al.* The retinitis pigmentosa GTPase regulator (RPGR) interacts with novel transport-like proteins in the outer segments of rod photoreceptors. *Hum. Mol. Genet.* **9**, 2095–2105 (2000).
8. Dryja, T.P. *et al.* Null *RPGRIP1* alleles in patients with Leber congenital amaurosis. *Am. J. Hum. Genet.* **68**, 1295–1298 (2001).
9. Satran, D., Pierpont, M.E. & Dobyns, W.B. Cerebello-oculo-renal syndromes including Arima, Senior-Loken and COACH syndromes: more than just variants of Joubert syndrome. *Am. J. Med. Genet.* **86**, 459–469 (1999).
10. Parisi, M.A., Doherty, D., Chance, P.F. & Glass, I.A. Joubert syndrome (and related disorders) (OMIM 213300). *Eur. J. Hum. Genet.* **15**, 511–521 (2007).
11. Maria, B.L. *et al.* Molar tooth sign in Joubert syndrome: clinical, radiologic, and pathologic significance. *J. Child Neurol.* **14**, 368–376 (1999).
12. Pellegrino, J.E., Lensch, M.W., Muenke, M. & Chance, P.F. Clinical and molecular analysis in Joubert syndrome. *Am. J. Med. Genet.* **72**, 59–62 (1997).
13. Ferland, R.J. *et al.* Abnormal cerebellar development and axonal decussation due to mutations in AHI1 in Joubert syndrome. *Nat. Genet.* **36**, 1008–1013 (2004).
14. Baala, L. *et al.* The Meckel-Gruber syndrome gene, *MKS3*, is mutated in Joubert syndrome. *Am. J. Hum. Genet.* **80**, 186–194 (2007).
15. Fliegauf, M. *et al.* Nephrocystin specifically localizes to the transition zone of renal and respiratory cilia and photoreceptor connecting cilia. *J. Am. Soc. Nephrol.* **17**, 2424–2433 (2006).
16. Valente, E.M. *et al.* Mutations in *CEP290*, which encodes a centrosomal protein, cause pleiotropic forms of Joubert syndrome. *Nat. Genet.* **38**, 623–625 (2006).
17. Dawe, H.R. *et al.* The Meckel-Gruber Syndrome proteins MKS1 and meckelin interact and are required for primary cilium formation. *Hum. Mol. Genet.* **16**, 173–186 (2007).
18. Chang, B. *et al.* In-frame deletion in a novel centrosomal/ciliary protein CEP290/NPHP6 perturbs its interaction with RPGR and results in early-onset retinal degeneration in the rd16 mouse. *Hum. Mol. Genet.* **15**, 1847–1857 (2006).
19. Otto, E. *et al.* A gene mutated in nephronophthisis and retinitis pigmentosa encodes a novel protein, nephroretinin, conserved in evolution. *Am. J. Hum. Genet.* **71**, 1161–1167 (2002).
20. Wolfrum, U. Centrin in the photoreceptor cells of mammalian retinae. *Cell Motil. Cytoskeleton* **32**, 55–64 (1995).
21. Rattner, A., Chen, J. & Nathans, J. Proteolytic shedding of the extracellular domain of photoreceptor cadherin. Implications for outer segment assembly. *J. Biol. Chem.* **279**, 42202–42210 (2004).
22. Banizs, B. *et al.* Dysfunctional cilia lead to altered ependyma and choroid plexus function, and result in the formation of hydrocephalus. *Development* **132**, 5329–5339 (2005).
23. Doolin, P.F. & Birge, W.J. Ultrastructural organization of cilia and basal bodies of the epithelium of the choroid plexus in the chick embryo. *J. Cell Biol.* **29**, 333–345 (1966).
24. Ramensky, V., Bork, P. & Sunyaev, S. Human non-synonymous SNPs: server and survey. *Nucleic Acids Res.* **30**, 3894–3900 (2002).
25. Ng, P.C. & Henikoff, S. Predicting deleterious amino acid substitutions. *Genome Res.* **11**, 863–874 (2001).
26. Kantardzhieva, A. *et al.* MPP5 recruits MPP4 to the CRB1 complex in photoreceptors. *Invest. Ophthalmol. Vis. Sci.* **46**, 2192–2201 (2005).
27. Roepman, R., Schick, D. & Ferreira, P.A. Isolation of retinal proteins that interact with retinitis pigmentosa GTPase regulator by interaction trap screen in yeast. *Methods Enzymol.* **316**, 688–704 (2000).
28. van Wijk, E. *et al.* The *DFNB31* gene product whirlin connects to the Usher protein network in the cochlea and retina by direct association with USH2A and VLGR1. *Hum. Mol. Genet.* **15**, 751–765 (2006).
29. Brandstatter, J.H., Koulen, P., Kuhn, R., van der, P.H. & Wassle, H. Compartmental localization of a metabotropic glutamate receptor (mGluR7): two different active sites at a retinal synapse. *J. Neurosci.* **16**, 4749–4756 (1996).
30. Mogensen, M.M., Malik, A., Piel, M., Bouckson-Castaing, V. & Bornens, M. Micro-tubule minus-end anchorage at centrosomal and non-centrosomal sites: the role of ninein. *J. Cell Sci.* **113**, 3013–3023 (2000).